M1 Mirror Alignment in BWG Antennas with Connected-Element Interferometry Holography

Manuel Vazquez*, Alberto Torre*, and David Rochblatt†

ABSTRACT. — Computer simulation is a very active field in many branches of science. It allows for the prediction of the behavior of many systems without the cost and time of an actual experiment. In this paper, we describe a simulator of a dual-shaped paraboloidal reflector antenna and the use of it to assist in the alignment of the M1 flat mirror in a beam-waveguide (BWG) antenna (particularly DSS-55). The predicted correction was then corroborated by measurements in the field. The simulator generates the far field for a certain deviation of a feed placed at F1, and then the far field is translated to the aperture of the antenna by means of the holography data processing software. The simulations are guided by the data collected with the holography that are then compared to predict the M1 correction.

I. Introduction

BWG mirror alignment is an involved task that is done mainly at the commissioning of the antenna. The microwave mirrors are manufactured with a central section that can be removed and then replaced by a mirror that can reflect a red-light laser. These mirrors can also, from a telescope installed at the center of the M5 mirror, check the alignment of the subsequent mirrors by setting the telescope focus at different distances. This technique aligns the mirrors with enough accuracy to properly set the F3 focus coincident with the feed focus at the pedestal. The last mirror, M1, is set by sending the laser to the center of the subreflector that reflects the laser and sends it back to the M1 mirror. This final alignment relies on a proper subreflector alignment with the main dish, which is not always the case. The main indication of the optical alignment of a BWG antenna as a whole is the illumination and the phase of the

*Madrid Deep Space Communication Complex, MDSCC

†JPL

The research described in this publication was carried out by the Jet Propulsion Laboratory, California Institute of Technology, under a contract with the National Aeronautics and Space Administration.

aperture measured at F3. The aperture field can be measured for different positions of the antenna, and hence, different mirror rotations with connected-element interferometry (CEI) holography [1]. The variation of the aperture field can assist the mirror alignment personnel to determine which mirror is more likely to be misaligned. Once the mirrors between and including M5 to M2 have been aligned, the final step can be performed with the assistance of CEI holography and the simulator. DSS-55 presented, after having several mechanical problems in the holding structure of the mirrors, a severe degradation of the aperture illumination. The subreflector correction also gave inconsistent values depending on the position of the antenna. All together, this suggested a misalignment problem in one or more mirrors. This paper describes the simulator that was used for this task with a description of how the dual shape was generated. Next there is a brief description about BWG antennas and how we match CEI holography results with simulated apertures. Finally, there is a description of how M1 was aligned using this technique and a discussion about the particular case of DSS-55.

II. Antenna Simulator

A. Radiated field

The antenna simulator has been developed under physical optics (PO) theory. The algorithm is based on adding the vectors of the impulse responses of all the source currents on the antenna surface. The impulse responses of the sources are expressed as [2]:

$$\boldsymbol{E_{le}}(\boldsymbol{r},\boldsymbol{r'},\boldsymbol{J}(\boldsymbol{r'})) = -G_{EJ}(\boldsymbol{r},\boldsymbol{r'}).\boldsymbol{J}(\boldsymbol{r'}) \tag{1}$$

$$\boldsymbol{E_{lm}}(\boldsymbol{r},\boldsymbol{r'},\boldsymbol{M}(\boldsymbol{r'})) = -G_{EM}(\boldsymbol{r},\boldsymbol{r'}).\boldsymbol{M}(\boldsymbol{r'}) \tag{2}$$

$$\boldsymbol{H_{le}}(\boldsymbol{r},\boldsymbol{r'},\boldsymbol{J}(\boldsymbol{r'})) = -G_{HJ}(\boldsymbol{r},\boldsymbol{r'}).\boldsymbol{J}(\boldsymbol{r'}) \tag{3}$$

$$\boldsymbol{H_{lm}}(\boldsymbol{r},\boldsymbol{r'},\boldsymbol{M}(\boldsymbol{r'})) = -G_{HM}(\boldsymbol{r},\boldsymbol{r'}).\boldsymbol{M}(\boldsymbol{r'}) \tag{4}$$

where subscript l relates to the impulse response and

G_{xx} are the dyadic quantities (Green's functions)
E is the electric field
H is the magnetic field
J is the electric current
M is the magnetic current

The radiated electromagnetic fields are obtained by

$$\boldsymbol{E}(\boldsymbol{r}) = -\int G_{EJ}(\boldsymbol{r},\boldsymbol{r'}).\boldsymbol{J}(\boldsymbol{r'})dV' - \int G_{EM}(\boldsymbol{r},\boldsymbol{r'}).\boldsymbol{M}(\boldsymbol{r'})dV' \tag{5}$$

$$\boldsymbol{H}(\boldsymbol{r}) = -\int G_{HJ}(\boldsymbol{r},\boldsymbol{r'}).\boldsymbol{J}(\boldsymbol{r'})dV' - \int G_{HM}(\boldsymbol{r},\boldsymbol{r'}).\boldsymbol{M}(\boldsymbol{r'})dV' \tag{6}$$

The simulator is implemented in software with vector propagators that calculate radiated fields from source distributions. This particular implementation of this theory for reflector surfaces performs very well. The reflected fields are calculated by finding the PO currents on the reflecting surface and reradiating them to the next surface. The simulator implements a corrugated feed horn and a dual reflector Cassegrain geometry. This configuration is used by the DSN to increase the effective "focal length" of a parabolic main reflector without increasing its size.

B. Geometry

The geometry of the Cassegrain system is generated as a dual-shaped reflector to obtain a uniform aperture illumination to increase the efficiency. The dual shape is achieved by representing the reflector by a sequence of conic sections with the algorithm described in [3]. This is an iterative process that progresses with θ_{Fn} in which n passes through all values from 0 to θ_E, which is the half-subtended angle (rads) of the subreflector as seen from the feed in steps of $\Delta_T = 0.01 * pi/180$.

The full geometry is generated by the revolution of the section generated by the algorithm. The final 3D geometry is shown in Figure 1.

The simulator can analyze the optical system with several degrees of freedom:

- The subreflector can tilt in two axes and can displace in three axes.

- The feed placed in F1 (vertex of the main dish) can rotate in two axes and can displace in three axes.

For a certain configuration we can generate the far field of the antenna, which has the

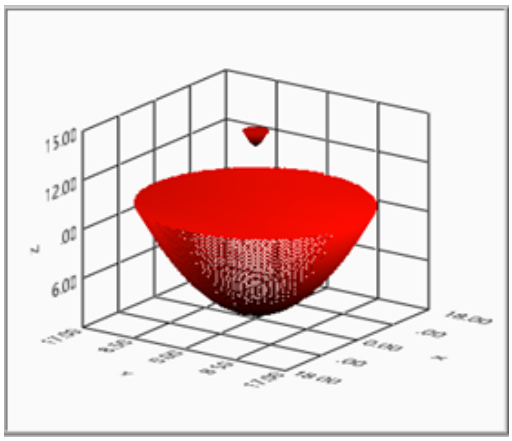

Figure 1. Dual-shape geometry.

following expression [4]:

$$T(u,v) = -\int J(x,y)e^{jkz}e^{jk(ux+vy)}dxdy \tag{7}$$

where $J(x,y)$ is the induced surface current defined as $J = 2n \times H$,

can be reexpressed as [5]:

$$T(u,v) = -\int Q(x,y)e^{jkz}e^{jk(ux+vy)}dxdy \tag{8}$$

where Q is a function that is zero outside the reflector, then the Fourier transform holds.

The function Q is constructed from T using the relation [6]:

$$Q(x,y) = F^{-1}[T] \tag{9}$$

Q is precisely the illumination function at the aperture plane. The far field measured by the holography system may be improved in resolution by filling with zeros beyond the field limits and, by an iterative process, obtain the function Q. Parseval's theorem can be used to show that the tail of Q(x,y) gradually diminishes.

The far field can be generated in Cartesian or polar topology, and hence, different coordinates for the far field are used. The inverse Fourier transform algorithm is different in both cases but yields to same results [7].

III. BWG Antennas

A BWG feed system is composed of one or more feeds along with several mirrors that can be flat or curved. The resultant optical system can propagate the energy from or to the feed through the mirrors.

A DSN BWG feed system (Figure 2) is composed of two ellipsoidal mirrors (M2 and M3), two flat mirrors (M1 and M4), and one ellipsoidal mirror within the shroud (M5)[8].

The alignment of this optical system, from F1 placed near the vertex of the main dish to F3 in the feed, is done with mechanical techniques. It is a task that must be done in a thermally stable environment and requires skill and time. The detailed description of the mirror alignment is outside the scope of this paper and can be visited in the DSN-related documentation.

The purpose of this analysis is to present an alternative technique to perform the final adjustment of M1 that serves as the interface between the Cassegrain optical system formed by the main reflector and the subreflector, and the BWG system formed by the curved and flat mirrors. In other words, F1 can be seen from the Cassegrain system or from the BWG system, and we must make both focal points coincident by adjusting M1 and the subreflector.

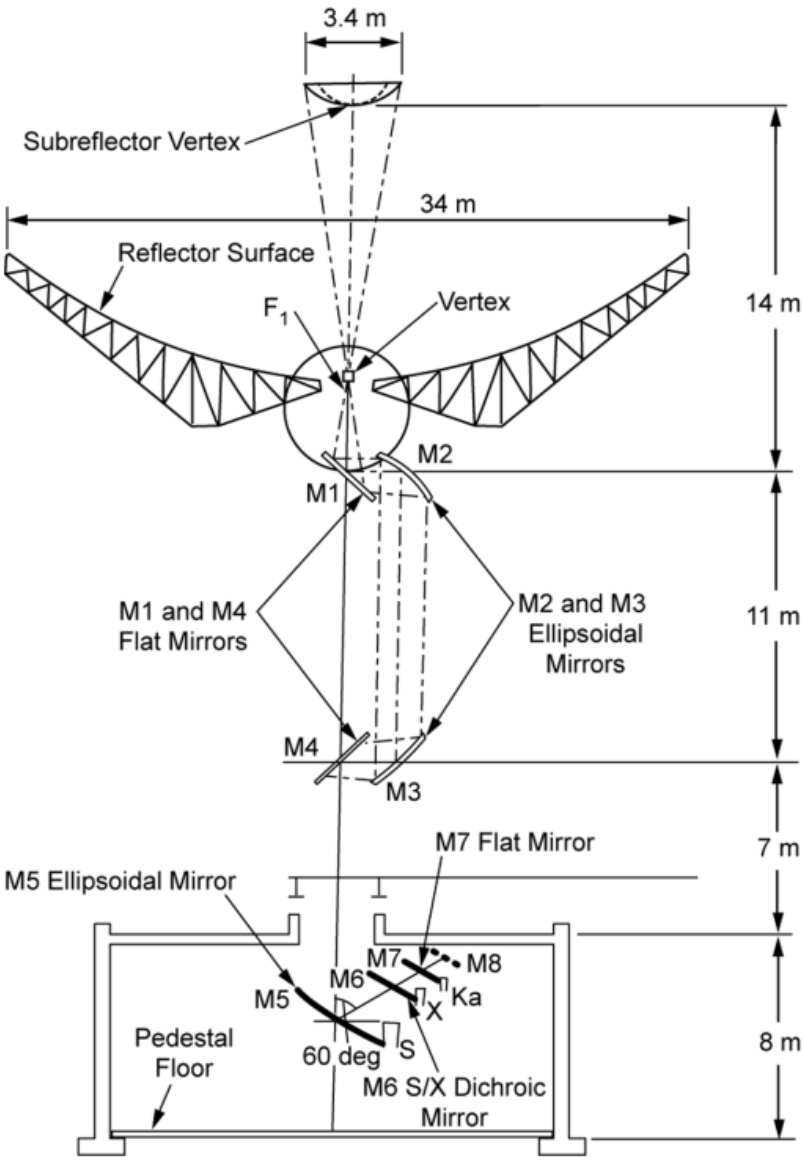

Figure 2. BWG antenna.

Figure 2 shows the operational DSN BWG antenna where F1 is placed above M1. F2, the image of F1 at the other end of the mirrors, is somewhere between M4 and M5. Below the floor, there is a magnifying ellipsoidal mirror (M5) that rotates to move the microwave beam to the different feed positions.

This technique is based on a comparison between data obtained from actual aperture measurements with the antenna under test and computer-generated simulations. The approximation is subject to a certain level of error, and it is interesting work for future development to automate the simulated and the acquired fitting.

IV. CEI Holography and Simulated Aperture

The CEI holography is well described in [1], which explains the method to determine the distribution of the aperture illumination and phase at a DSN operational frequency (X, Ka, K), hence, at the F3 position.

For a perfectly aligned system, these images should provide the typical aperture distribution for a dual-shaped system, which is the design used for the DSN reflectors to optimize the efficiency and minimize the spillover. The illumination is uniform with a sharp taper at the edge of -20 dB and a symmetric and almost uniform phase profile [9].

Figure 3 has been generated with the antenna simulator and the feed set at F1 perfectly aligned. The reflector at the left shows the amplitude profile of the aperture, and the reflector at the right shows the phase distribution. The normalized radiation function is [9]:

$$f(\theta,\phi) = \frac{d^2}{4}\int_0^1\int_0^{2\pi} F(r,\chi)e^{i\Phi(r,\chi)}e^{[-ik\frac{dr}{2}sin\theta cos(\chi-\phi)]}drd\chi \tag{10}$$

where $F(r,\chi)$ and $\phi(r,\chi)$ are the amplitude and phase terms of the illumination function. When we have a constant phase over the aperture and a rotationally symmetric illumination, the integral is

$$f(u) = \frac{\pi d^2}{2}\int_0^1 F(r)J_0(ur)rdr \tag{11}$$

where $J_0(u,r)$ is the Bessel function of the first kind and order zero, $u = \left(\frac{\pi d}{\lambda}\right)\sin\theta$ is the angular coordinate, and d is the diameter of the aperture. For a uniform aperture it yields to $f(u) = \frac{J_1(u)}{u}$.

If the antenna is defocused axially or laterally, the radiation pattern is influenced and hence the aperture changes from the uniformity presented before.

An axial defocus, resulting from a feed or subreflector displaced over the paraboloid axis, will cause a phase change over the aperture [9]:

$$\Delta\Phi(r) = \frac{2\pi\delta}{\lambda}(1 - cos\psi_0)r^2 \equiv \beta r^2 \tag{12}$$

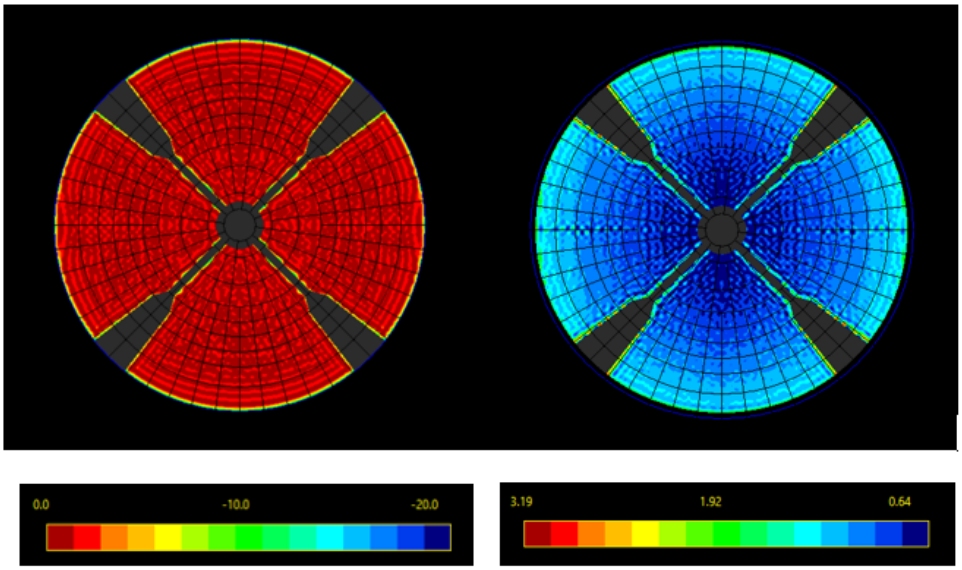

Figure 3. Aligned optics, left amplitude (dB) right phase (rad).

where ψ_0 is the opening half-angle of the paraboloid and δ is the axial defocus.

The power pattern can now be written as

$$U_1(u,\beta) = \frac{2\beta}{u} J_1(u) - \left(\frac{2\beta}{u}\right)^3 J_3(u) + \left(\frac{2\beta}{u}\right)^5 J_5(u) - ... \tag{13}$$

$$U_2(u,\beta) = \left(\frac{2\beta}{u}\right)^2 J_2(u) - \left(\frac{2\beta}{u}\right)^4 J_4(u) + ... \tag{14}$$

$$G(u,\beta) = \frac{1}{\beta^2}\left(U_1^2(u,\beta) + U_2^2(u,\beta)\right) = 4\left(\frac{J_1(u)}{u}\right)^2 - 16\beta^2\left(\frac{2J_1(u)J_3(u)}{u^4} - \frac{J_2^2(u)}{u^4}\right) + ... \tag{15}$$

Figure 4 shows the effect of an axial displacement over the aperture. The illumination shows very little effect, but the phase shows the quadratic dependency with the radius of the main reflector.

In the case of lateral defocus either from the feed or subreflector, the phase error will depend on the azimuthal aperture coordinate χ under the form

$$\Delta\Phi(r,\chi) = \frac{2\pi}{\lambda}\delta\frac{r}{f}\left(\frac{1}{1+\left(\frac{r}{2f}\right)^2}\right) cos\chi \tag{16}$$

This equation is valid for $\frac{\delta}{f} << 1$ where δ is the lateral defocus and f is the focal length.

The example in Figure 5 shows the effect in the aperture for a subreflector with a lateral defocus in X = +8 mm.

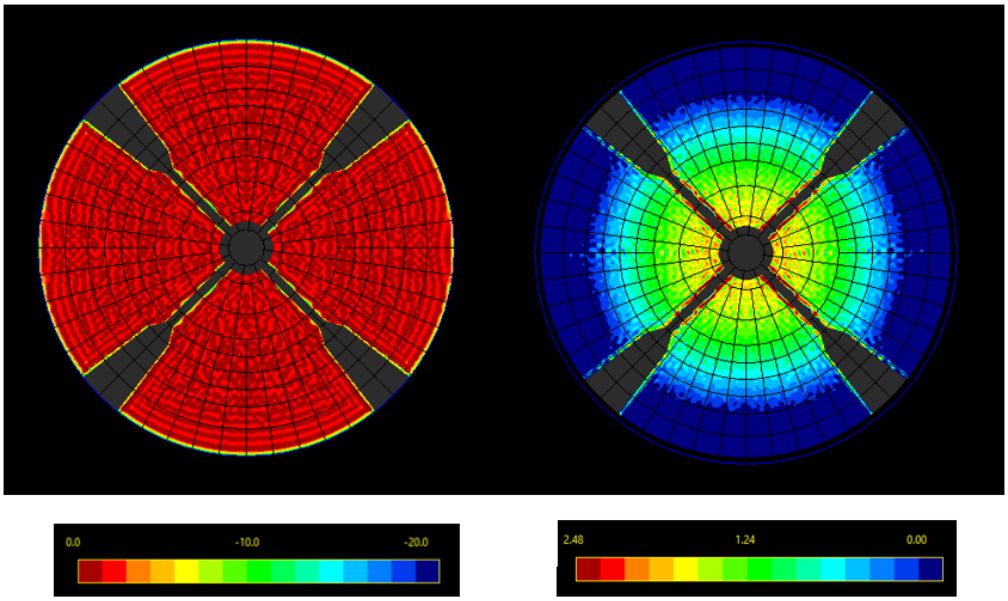

Figure 4. Axial displacement, left amplitude (dB) right phase (rad).

Existing literature shows the effects in the phase of the aperture illumination function caused by subreflector tilts and displacements, as well as feed displacements, e.g. [10]. However, no reference is made to the distortion in the illumination function caused by a tilt in the feed. This effect has been simulated, and the resulting illumination function shows a degradation in the amplitude but not in the phase. The feed tilt effect affects the amplitude distribution in the aperture as it squints the energy to one side. What is particular in this case is that the phase is practically not affected. The example in Figure 6 shows the amplitude squint for a tilt around the Y axis of 2 deg.

The aperture distribution, both in amplitude and phase resulting from our measurements, can be fitted from the combination of the described misfocuses. Whether they can be placed in the subreflector or in the feed and hence in M1 will depend on the proper analysis of the data.

V. M1 Alignment

The feed in our simulator is placed at F1 as it is shown in Figure 7. The distance between M1 mirror (flat) and F1 is 121.5 inches according to the DSN design.

The idea to translate an F1 placed feed misalignment to M1 misalignment is supported on the M1 design, which is a flat mirror. M1 has been designed with the purpose of reflecting the beam to illuminate the subreflector, but it does not change the beam optics. Actually, for the Gaussian beam design, Veruttipong[11] does not include M1 for the analysis, as seen in Figure 8.

Therefore we can treat F1 as the feed of the beam. Tilting M1 in both axes, pitch,

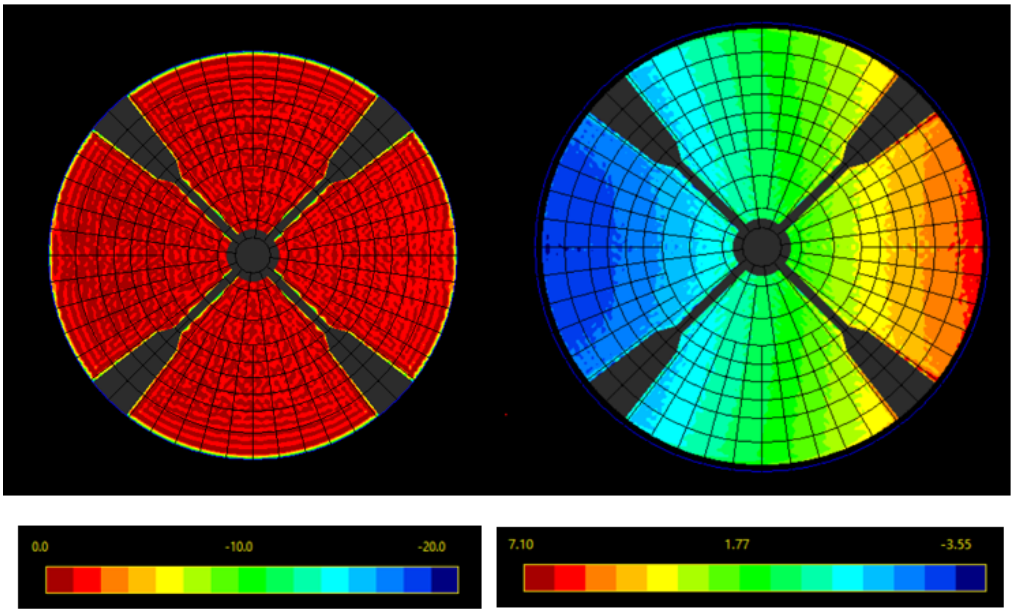

Figure 5. Lateral displacement (X=8 mm), left amplitude (dB) right phase (rad).

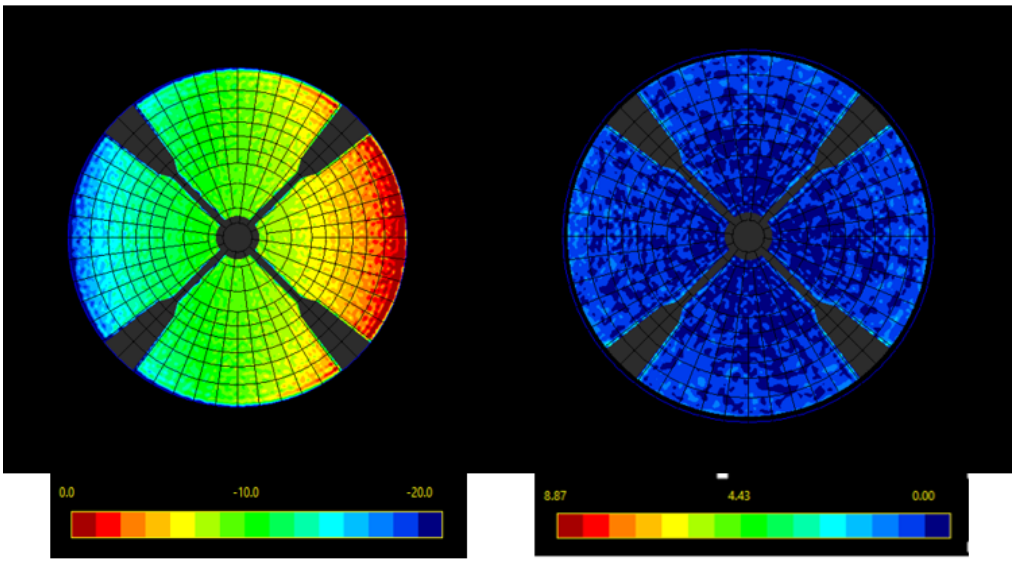

Figure 6. Feed tilt (Y=2 deg), left amplitude (dB) right phase (rad).

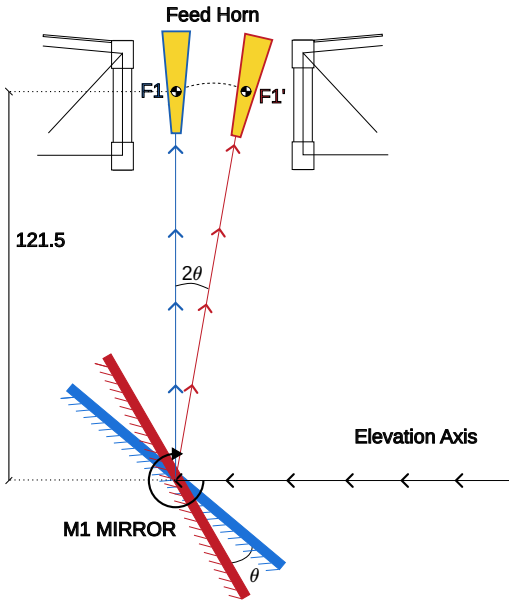

Figure 7. M1 vs F1 feed equivalence

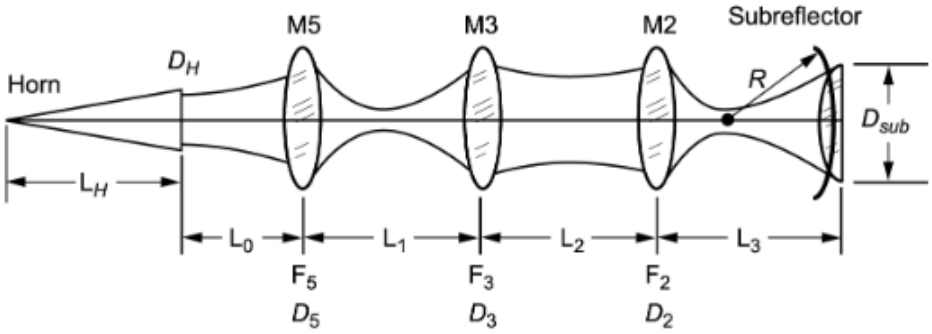

Figure 8. Gaussian beam design.

and roll, are reflected in F1 as a lateral displacement added to a beam tilt as seen in Figure 7.

According to Snell's law the ratio between the feed tilt and the mirror tilt is:

$$\alpha_{Mirror} = \frac{\alpha_{Feed}}{2} \tag{17}$$

$$\delta_{Feed} = \alpha_{Feed} * 121.5(inch) \tag{18}$$

At DSS-55 the alignment proceeded from the horn at the pedestal up to M1. The support of lasers included in topographic total stations and telescopes installed in the center of the mirrors allowed for successful alignment from M5 to M2. M1 was subject to the same alignment process with the subreflector as it was supposed to be centered with the main dish. This last operation was not successful, and then the aperture analysis was used for the final M1 alignment.

VI. DSS-55 Measurements

DSS-55 lost more than 3 dB of gain in Ka band between 2017 and 2018. From the very beginning, the problem was suspected to be the mirrors but there were no radiometric tools to clearly diagnose the issue. Later on, marks inside the BWG tube indicated that at least one mirror collapsed from its original position. After a detailed mechanical analysis in 2018, there was a campaign to realign the mirrors, and part of the efficiency was recovered but the problem was not completely fixed. The problem was finally addressed in 2023 with full mirror alignment from the feed at the pedestal to M1. The efficiency was recovered to the value from the beginning of 2017. During this final alignment campaign, M1 was aligned using holography images and the full antenna optics validated with radiometric techniques.

Before the alignment process, a baseline measurement was done to assess the status of the antenna. The measurement had a double purpose:

- Evaluate the level of misalignment of the mirrors
- Evaluate the impact of such misalignment on the gain of the antenna

The efficiency profile of the antenna was severely affected. See Figure 9 where it shows the efficiency of the antenna while tracking 3C274. The efficiency was higher for azimuth angles toward the west, which suggested a mirror misalignment dependent on the azimuth of the antenna. Several CEI holography measurements were done at different azimuths and elevations (Table 1), which resulted in the illumination apertures shown in Figure 10.

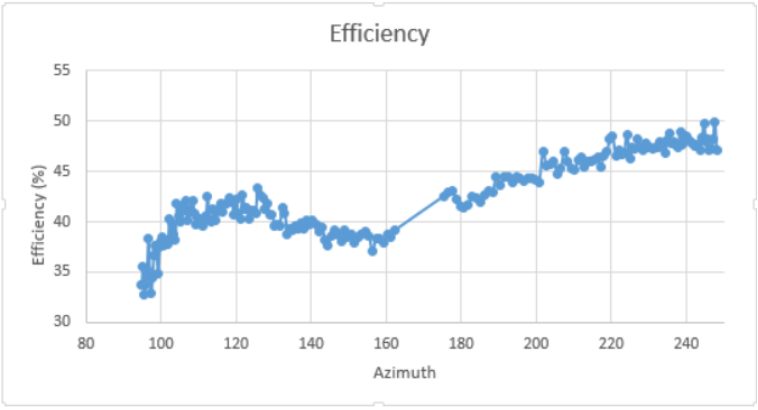

Figure 9. Efficiency baseline measurement.

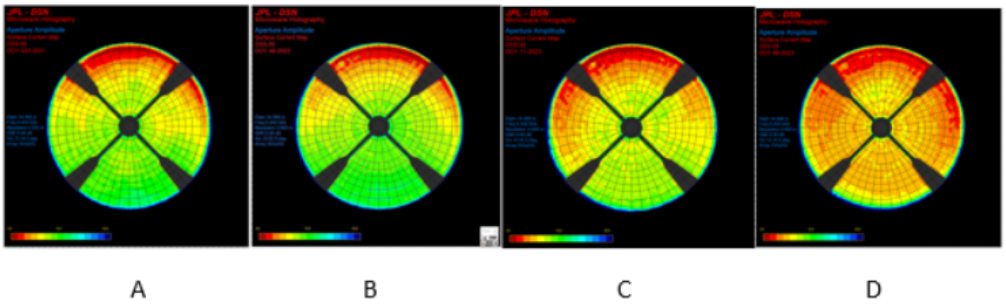

Figure 10. Illumination maps for different antenna positions.

Table 1. Antenna positions for illumination maps.

Position	A	B	C	D
Azimuth	60	136	190	270
Elevation	30	55	50	40

For eastern azimuth angles, the integrated illumination and the efficiency are lower. As we move to the west, the integrated illumination and efficiency both improve. This proves the dependency between the illumination profile and the efficiency of the antenna.

M5 to M2 were aligned in several steps, and the final iteration was done completely based on aperture analysis on CEI holography images. The basic idea of this technique is to extract from the aperture data what is common for all the antenna positions and can be corrected with M1 alignment. The residual part can be corrected either in the subreflector or it is a remnant misalignment in one of the other mirrors.

For M1-subrefector (SR) alignment, three CEI holography measurements were performed at different positions as shown in Table 2.

Table 2. Antenna positions for illumination and phase maps.

Position	A	B	C
Azimuth	110	245	275
Elevation	55	57	27

For every position, and from the far field measurement, the holography data processing system generates the aperture illumination and phase maps. The software inputs these data to the optimum paraboloid defined by six parameters or degrees of freedom: three translations, two rotations, and the focal length. These parameters are translated to the subreflector by means of M (magnification factor) as subreflector corrections[4][12]. For antennas with the feed in the primary focus, these corrections may indicate a subreflector misalignment or a feed misalignment, but for BWG antennas, this misalignment may be present in any of the subsequent mirrors. The problem, then, must be compartmentalized. In the case of DSS-55, M5 to M2 had been previously aligned so any residual misalignment must be between M1 and the subreflector. For two of the three positions, several simulations were performed and the solution was chosen that best matched the aperture maps and the subreflector computed corrections generated by the CEI holography measurements. Figure 11 shows the illumination and phase for the aperture at position A from Table 2, and Figure 13 shows the illumination and phase for the aperture at position B. The subreflector corrections are included in Table 3 for position A and Table 5 for position B.

After trial and error, the simulation parameters that best matched the aperture at positions A and B are the following:

Position A:

Feed shift in X: 5.3 cm, Feed tilt CW: 1 deg, SR bias in X axis: 4 mm

Position B:

Feed shift in X: 4.5 cm, Feed tilt CW: 0.7 deg, SR bias in X axis: 4 mm

The apertures for these simulations are shown in Figures 12 and 14, and the subreflector corrections are included in Tables 4 and 6 respectively.

Note that, as the amplitude is degraded for positions A and B, a feed tilt is required in the simulation. The value of the tilt required in the simulation to match the real holography measurements in positions A and B is 1 degree and 0.7 degree, respectively.

Notice how the illumination in Figure 12 (simulation) matches the illumination in Figure 11 (real), and the illumination in Figure 14 (simulation) matches the illumination in Figure 13 (real).

A quick analysis of the simulation parameters shows that:

There is a consistent misalignment in the subreflector of +10 mm correction in the X axis and -0.4 deg in the Y axis tilt. This misalignment is reported both in the holography measurement and in the simulation.

The simulation can allocate the total misalignment into three parameters: a feed tilt, a feed displacement, and a subreflector misalignment. The feed tilt and feed displacement, as seen in Figure 7, can be explained together with a M1 tilt in the proper direction given that:

- Beam tilt of 0.7 deg shifts F1 by 3.8 cm
- Beam tilt of 1 deg shifts F1 by 5.38 cm

Both of these are in good agreement with the numbers generated by the simulation. These measurements suggests an M1 tilt in the opposite direction to correct the aperture plus an X correction in the subreflector.

The M1 correction for these numbers is half of the beam tilt, which is 0.35 deg for simulation A and 0.5 deg for simulation B. The DSS-55 mirror alignment team agreed on a conservative correction of 0.25 deg given that the mechanical correction of M1 does not allow for a precise tilt movement and can be easily over corrected. The correction applied to the subreflector was 3 mm in the X axis.

After the mirror correction, there was a CEI holography measurement to check the aperture phase and illumination and the new subreflector corrections. This measurement was done with 3C84 at azimuth 75 deg and elevation 80 deg; see Figure 15 showing the aperture illumination and phase, and Table 7 showing the subreflector corrections. Note that these corrections are lower than before the M1 tilt, especially the X-axis. Figure 15 shows how after applying the correction to M1, the amplitude became uniform across the aperture plane.

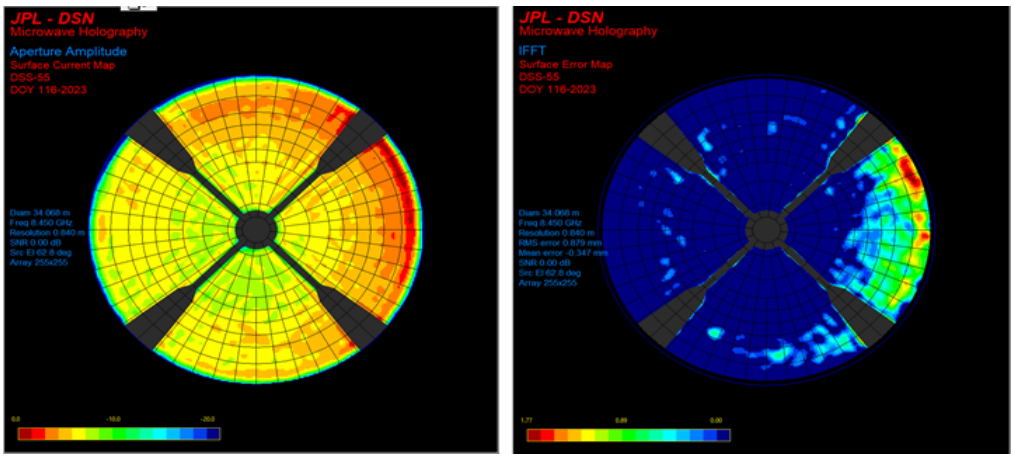

Figure 11. Position A aperture, left amplitude (dB) right phase (rad).

Table 3. Subreflector corrections for position A.

$X - Translation(mm)$	9.39
$Y - Translation(mm)$	1.69
$Z - Translation(mm)$	-0.02
$X - AxisTilt(deg)$	0.09
$Y - AxisTilt(deg)$	-0.51

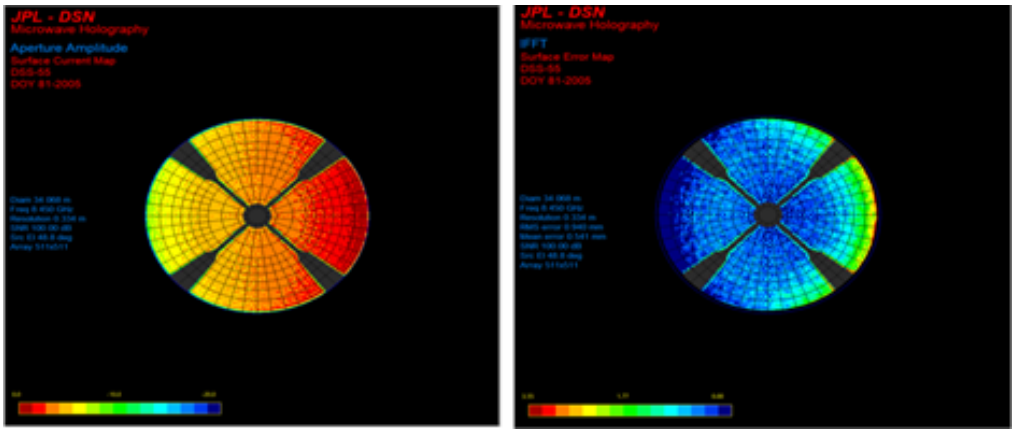

Figure 12. Simulation for Position A aperture, left amplitude (dB) right phase (rad).

Table 4. Subreflector corrections for position A in simulation.

$X - Translation(mm)$	9.52
$Y - Translation(mm)$	0.1
$Z - Translation(mm)$	0.025
$X - AxisTilt(deg)$	0.003
$Y - AxisTilt(deg)$	-0.51

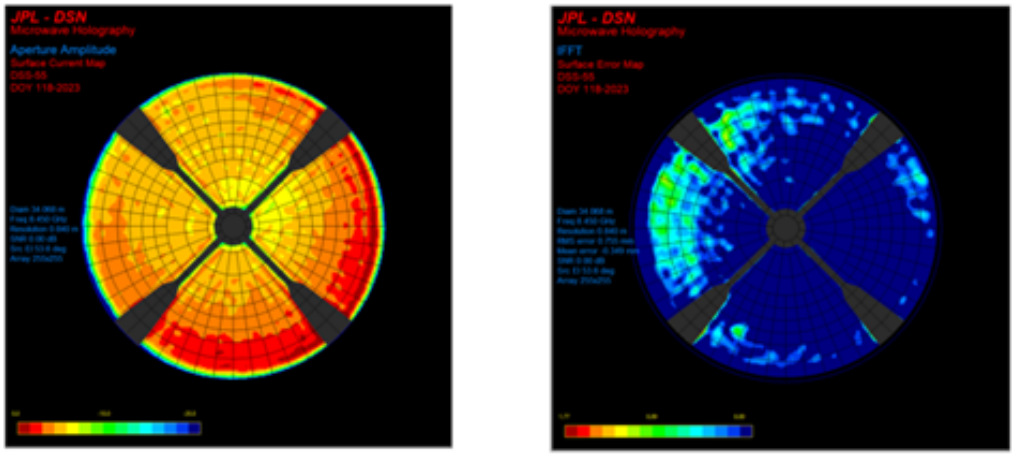

Figure 13. Position B aperture, left amplitude (dB) right phase (rad).

Table 5. Subreflector corrections for position B.

$X - Translation(mm)$	9.14
$Y - Translation(mm)$	-3.72
$Z - Translation(mm)$	-0.04
$X - AxisTilt(deg)$	-0.15
$Y - AxisTilt(deg)$	-0.41

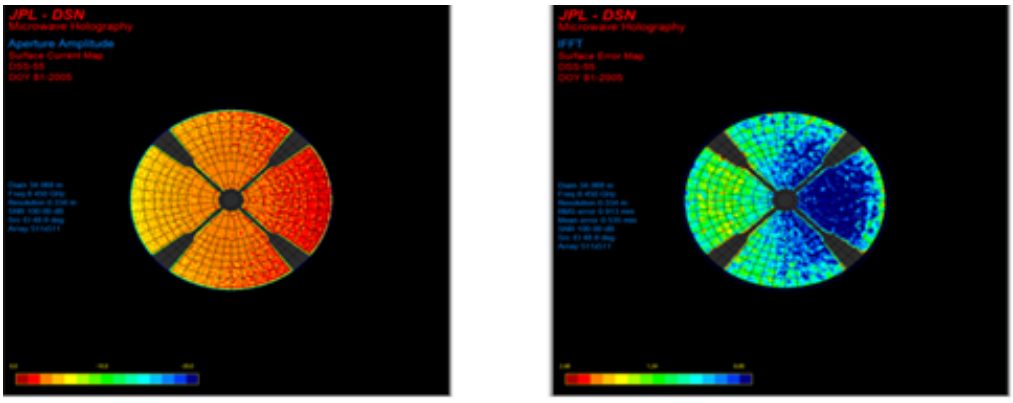

Figure 14. Simulation for Position B aperture, left amplitude (dB) right phase (rad).

Table 6. Subreflector corrections for position B in simulation.

$X - Translation(mm)$	9.24
$Y - Translation(mm)$	0.05
$Z - Translation(mm)$	0.025
$X - AxisTilt(deg)$	0.003
$Y - AxisTilt(deg)$	-0.39

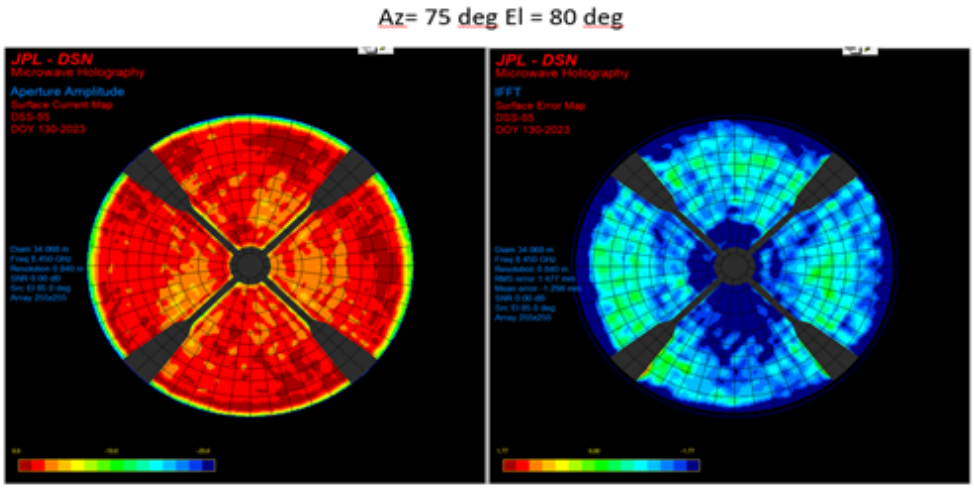

Figure 15. Check after M1 tilt, left amplitude (dB) right phase (rad).

Table 7. Subreflector corrections after M1 tilt correction.

$X - Translation(mm)$	-0.97
$Y - Translation(mm)$	-2.85
$Z - Translation(mm)$	0.6
$X - AxisTilt(deg)$	-0.13
$Y - AxisTilt(deg)$	0.04

For a final check, the efficiency and gain of the antenna were measured with 3C274 with two purposes:

- Verify that the efficiency is back to the level previous to the mirror misalignment.

- Check that the peak of the efficiency is the same between east and west.

Figures 16 and 17 repectively show the efficiency and gain versus elevation for the rise (east) and set (west) of 3C274.

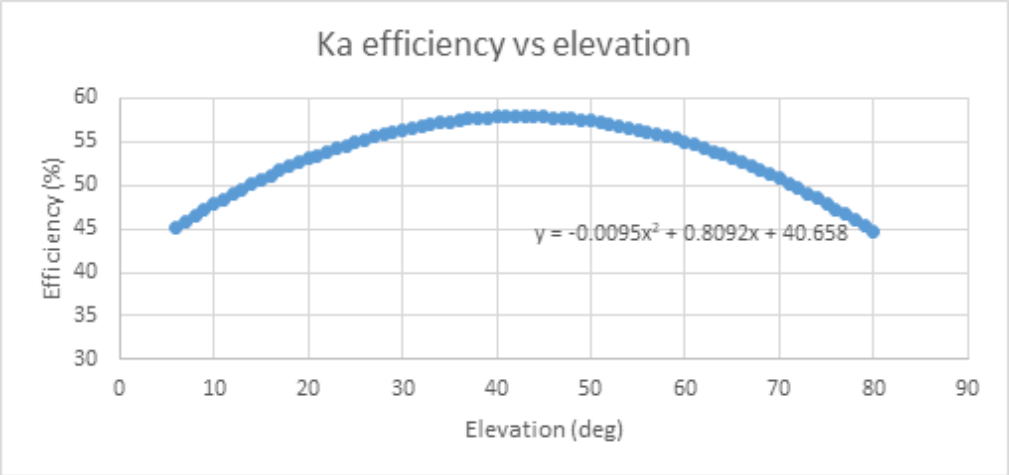

Figure 16. Ka efficiency (in percent) vs elevation.

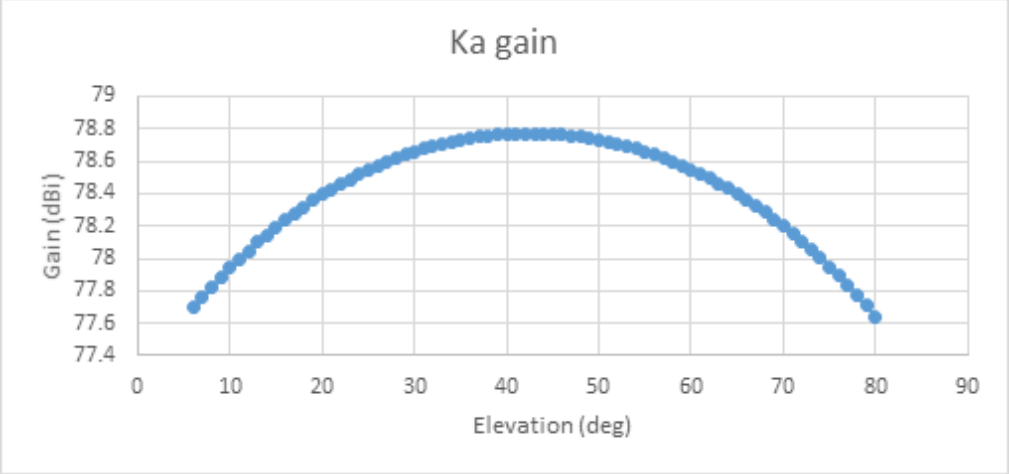

Figure 17. Ka gain vs elevation.

It is important to note that the agreement between the measured aperture images and the simulated ones is based on visual observation and then, subject to individual biases and quantitative errors.

VII. Conclusions

The optical design of the BWG antennas is much more complex than the dual-reflector antennas. This is the price to pay for the simplicity in the installation and maintenance (the electronics can be subject to corrective maintenance even during the operation of the antenna). As a result of this complexity, the alignment is a delicate process during the commissioning of the antenna, and its final performance depends completely on it. The optics system of the antenna can be divided into two

parts. One belongs to the reflector-subreflector pair that concentrates the energy in F1, and it is the subject of the simulation presented here. The other part is the system formed by the curved mirrors (M2, M3, and M5) that replicates F1 downstream to F3. M1 and M4 are just plain mirrors to reflect the energy in the proper direction [13]. F1 is the main focus of the reflector-subreflector, and it is the replication of the feed focus placed at F3 as well. The final and most important step in the alignment process is to make an agreement between the F1 or main focus of the dual reflector that is properly set during the F1 holography with the F1 as "seen" from the feed (F3) upstream. This agreement is the purpose of the technique developed during the DSS-55 downtime. Although the whole process was done by visual comparison of the measured and generated apertures, it is the holography development team's goal to automate the fitting with some kind of regression technique in the future. Extending this M1 alignment technique to the other mirrors is an active discussion within the antenna calibration team as a future development.

Acknowledgments

The authors want to thank MDSCC antenna staff (mechanics and servo) for their support during this task. Special thanks to David Muñoz, Rafael Romero, and Luis Neira. We would also like to thank John Cucchissi and Lisa Locke from JPL for supporting the use of this technology to calibrate BWG antenna optics.

References

[1] A. Torre and M. Vazquez, "Connected-element interferometer holography via correlation of signals from the common platform," *The Interplanetary Network Progress Report*, vol 42-241, Jet Propulsion Laboratory, Pasadena, California, pp. 1-19, May 15, 2025.

[2] L. Diaz and T. Milligan, *Antenna Engineering Using Physical Optics*. Artech House Publishers, Norwood, Massachussets, 1996.

[3] F. J. S. Moreira and J. R. Bergmann, "Shaping axis-symmetric dual-reflector antennas by combining conic sections," *IEEE Transactions on Antennas and Propagation*, vol. 59, no. 3, 2011.

[4] D. J. Rochblatt and B. L. Seidel, "Microwave antenna holography," *IEEE Transactions on Microwave Theory and Techniques*, vol. 40, no. 6, 1992.

[5] Y. Rahmat-Samii, "Surface diagnosis of large reflector antennas using microwave holographic metrology: An iterative aproach," *Radio Science*, vol. 19, no. 5, 1984.

[6] D. J. Rochblatt, "Holographic measurements of the NASA-JPL Deep Space Network antennas," *IEEE Aerospace Conference Proceedings*, 1998.

[7] A. Torre and M. Vazquez, "Connected-element interferometry holography with polar sampling," *The Interplanetary Network Progress Report*, vol 42-241, Jet Propulsion Laboratory, Pasadena, California, pp. 1-15, May 15, 2025.

[8] W. Imbriale, *Large Antennas of the Deep Space Network*. John Wiley & Sons, Inc., Hoboken, New Jersey, 2003.

[9] J. Baars, *The Paraboloid Reflector Antenna in Radio Astronomy and Communication*. Springer Science+Business Media, LLC, New York, New York, 2007.

[10] B. J. Butler, "Requirements for subreflector and feed positioning for ALMA antennas," *ALMA Memo No. 479*, 2003.

[11] W. Veruttipong, J. C. Chen, and D. Bathker, "Gaussian beam and physical optics iteration technique for wideband beam waveguide feed design," *The Telecommunications and Data Acquisition Report*, vol. 42-105, pp. 128-135, May 15, 1991.

[12] Y. Rahmat-Samii, "Microwave holography of large reflector antennas-simulation algorithms," *IEEE Transactions on Antennas and Propagations*, vol. AP-33, no. 11, 1985.

[13] T. Veruttipong, J. Withington, V. Galindo-Israel, W. Imbriale, and D. Bathker, "Design considerations for the beam-waveguide retrofit of a ground antenna station," *The Telecommunications and Data Acquisition Report*, vol. 42-87, pp. 10-23, November 15, 1986.